Chemical Science

EDGE ARTICLE

View Article Online
View Journal

CrossMark click for updates

Cite this: DOI: 10.1039/c5sc04652a

[Ni^{III}(OMe)]-mediated reductive activation of CO_2 affording a Ni(κ^1-OCO) complex†

Tzung-Wen Chiou,*[a] Yen-Ming Tseng,[a] Tsai-Te Lu,[b] Tsu-Chien Weng,[c] Dimosthenes Sokaras,[c] Wei-Chieh Ho,[a] Ting-Shen Kuo,[d] Ling-Yun Jang,[e] Jyh-Fu Lee[e] and Wen-Feng Liaw*[a]

Received 3rd December 2015
Accepted 16th February 2016

DOI: 10.1039/c5sc04652a

www.rsc.org/chemicalscience

Carbon dioxide is expected to be employed as an inexpensive and potential feedstock of C_1 sources for the mass production of valuable chemicals and fuel. Versatile chemical transformations of CO_2, *i.e.* insertion of CO_2 producing bicarbonate/acetate/formate, cleavage of CO_2 yielding μ-CO/μ-oxo transition-metal complexes, and electrocatalytic reduction of CO_2 affording CO/HCOOH/CH_3OH/CH_4/C_2H_4/oxalate were well documented. Herein, we report a novel pathway for the reductive activation of CO_2 by the [Ni^{III}(OMe)(P(C_6H_3-3-$SiMe_3$-2-S)$_3$)]$^-$ complex, yielding the [Ni^{III}(κ^1-OCO$^{\bullet-}$)(P(C_6H_3-3-$SiMe_3$-2-S)$_3$)]$^-$ complex. The formation of this unusual Ni^{III}(κ^1-OCO$^{\bullet-}$) complex was characterized by single-crystal X-ray diffraction, EPR, IR, SQUID, Ni/S K-edge X-ray absorption spectroscopy, and Ni valence-to-core X-ray emission spectroscopy. The inertness of the analogous complexes [Ni^{III}(SPh)], [Ni^{II}(CO)], and [Ni^{II}(N_2H_4)] toward CO_2, in contrast, demonstrates that the ionic [Ni^{III}(OMe)] core attracts the binding of weak σ-donor CO_2 and triggers the subsequent reduction of CO_2 by the nucleophilic [OMe]$^-$ in the immediate vicinity. This metal–ligand cooperative activation of CO_2 may open a novel pathway promoting the subsequent incorporation of CO_2 in the buildup of functionalized products.

Open Access Article. Published on 24 February 2016. Downloaded on 06/05/2016 19:23:44.
This article is licensed under a Creative Commons Attribution 3.0 Unported Licence.

Introduction

Carbon dioxide, the waste from human activity embodying the nature of high thermodynamic stability and chemical inertness, is expected to be employed as an inexpensive and potential feedstock of C_1 sources for the regeneration of valuable chemicals and fuel.[1,2] Nature developed carbon monoxide dehydrogenase (CODH) to harbor a Ni–Fe cluster for the reversible interconversion between CO_2 and CO.[3–5] To gain insight into the mechanism for the conversion of CO_2 to CO in CODH, several Ni–CO_2 adducts derived from the reaction of a low-valent Ni complex and CO_2 were reported.[6–9] The direct electrochemical reduction of CO_2 affords oxalate, carbon monoxide, formic acid, methanol, methane, and ethylene.[10] To gain insight into the transformation of CO_2 at a molecular level, the chemistry of the activation of CO_2 *via* nucleophilic attack/interaction on the polarized C center, in addition to the reduction of the coordinated CO_2 ligand by low-valence transition metal complexes, has grown explosively over past years.[11] The versatile chemical transformations of CO_2, *i.e.* insertion of CO_2 producing bicarbonate/acetate/formate,[12–18] cleavage of CO_2 yielding μ-CO/μ-oxo transition-metal complexes,[19–23] reduction of CO_2 affording CO/HCOOH/CH_3OH/CH_4/C_2H_4/C_2H_6/methylene, and electrocatalysis of CO_2 converting it into oxalate, were well documented.[24–26] The direct electrochemical reduction or electrocatalytic transformation of CO_2 for the mass production of valuable chemicals and fuel, however, relies on the consumption of sustainable electric potential energy. Here we show a novel pathway for the reductive activation of CO_2 by a mononuclear Ni(III) complex [Ni^{III}(OMe)(P(C_6H_3-3-$SiMe_3$-2-S)$_3$)]$^-$.[27] This [Ni^{III}-(OMe)]-mediated reduction of CO_2 yields the complex Ni^{III}(κ^1-OCO$^{\bullet-}$), evidenced by single-crystal X-ray diffraction, EPR, SQUID, Ni/S K-edge X-ray absorption spectroscopy, IR and Ni valence-to-core X-ray emission spectroscopy. The ionic [Ni^{III}(OMe)] core provides a kinetic pathway to induce the binding of CO_2 and trigger the subsequent reduction of CO_2 by the nucleophilic [OMe]$^-$ in the immediate vicinity. The covalent [Ni^{III}(SPh)] core as well as Ni(II) center in complexes [Ni^{II}(L)(P(C_6H_3-3-$SiMe_3$-2-S)$_3$)]$^-$ (L = CO or N_2H_4), in contrast, are inert toward CO_2.[28]

[a]Department of Chemistry, National Tsing Hua University, Hsinchu, 30013, Taiwan. E-mail: d9623817@oz.nthu.edu.tw; wfliaw@mx.nthu.edu.tw
[b]Department of Chemistry, Chung Yuan Christian University, Taoyuan, 32023, Taiwan
[c]SLAC National Accelerator Laboratory, Menlo Park, CA 94025, USA
[d]Department of Chemistry, National Taiwan Normal University, Taipei, 10610, Taiwan
[e]National Synchrotron Radiation Research Center, Hsinchu, 30013, Taiwan

† Electronic supplementary information (ESI) available. CCDC 785531, 1435237 and 1435238. For ESI and crystallographic data in CIF or other electronic format see DOI: 10.1039/c5sc04652a

Results and discussion

Synthesis and characterization of nickel κ^1-OCO complex

When $CO_{2(g)}$ was bubbled into the thermally stable [Ni^{III}(OMe)(PS_3)]$^-$ (**1**) (PS_3 = P(C_6H_3-3-$SiMe_3$-2-S)$_3$) in THF,[27]

Open Access Article. Published on 24 February 2016. Downloaded on 06/05/2016 19:23:44.
This article is licensed under a Creative Commons Attribution 3.0 Unported Licence.

a pronounced color change from blue green to yellow green occurred to yield the O-bound κ^1-CO_2 complex $[Ni(\kappa^1\text{-}OCO)(PS_3)]^-$ (**2**), instead of complexes $[Ni(OC(O)OCH_3)\text{-}(PS_3)]^-$ or $[Ni(OC(O)H)(PS_3)]^-$ *via* the classical insertion or β-H migration mechanisms (Scheme 1a).[9,12–16]

The accompanied formation of [$^{\bullet}$OMe] in the reaction described above was corroborated using the spin-trapping reagent DMPO (ESI Fig. S1†).[29] The IR ν_{OCO} stretching peak at 2177 cm^{-1} (KBr) (ν_{OCO}: 2226 cm^{-1} in THF) exhibited by complex **2** supports the formation of $[Ni(\kappa^1\text{-}OCO)(PS_3)]^-$, which is consistent with the isotopic shift of the IR ν_{OCO} stretching peak to 2117 cm^{-1} (KBr) observed in the $^{13}CO_2$ labeling experiment (ESI Fig. S2†). The conversion of complex **1** to complex **2** under a CO_2 atmosphere was also monitored by UV-vis spectrometry; the intense bands at 419 and 605 nm disappeared with the simultaneous formation of absorption bands at 425 and 610 nm (THF) (ESI Fig. S3†). The green needle crystals of complex **2** were isolated when complex **2** was recrystallized from THF–diethyl ether at room temperature. As shown in Scheme 1b, treatment of complex **2** with $CO_{(g)}$ led to the formation of the reported complex $[Ni^{II}(CO)(PS_3)]^-$ accompanied by the release of $CO_{2(g)}$ characterized by IR and GC (Fig. 1).[28]

To contrast complex **2** containing a $[Ni^{III}\text{:}CO_2^{\bullet-}]$ or $[Ni^{II}\text{:}CO_2]$ center, complex $[Ni^{III}(NCO)(PS_3)]^-$ (**4**) was synthesized *via* the reaction of $[Ni(Cl)(PS_3)]^-$ (**3**) and [K][NCO] to mimic the isolobal $[Ni^{III}\text{:}CO_2]$ (Scheme 1c). Fig. 2 displays ORTEP plots of complexes **2** and **4**, with the selected bond distances and angles given in the caption. The strain effect of the chelating ligand ($[PS_3]^{3-}$) in the coordination sphere of complexes **2** and **4** explains that the Ni is in a distorted trigonal bipyramidal geometry with three thiolates locating equatorial positions and the phosphorus is occupying an axial position trans to the [OCO] and [NCO] ligands. In contrast to the linear N–C–O (177.2(3)°) bond observed in complex **4**, complex **2** displays a bent O–C–O bond with a bond angle of 171.7(7)°. Compared to the similar O–C and N–C bond distances of 1.200(3) and 1.181(3) Å in complex **4**, the dramatic difference (~0.1 Å) in O–C bond lengths, 1.132(6) *vs.* 1.240(7) Å, found in complex **2** moreover indicates the polarization of CO_2 *via* reductive activation affording a $[Ni^{III}\text{:}CO_2^{\bullet-}]$ species.[22,30,31] A similar polarization of CO_2 was reported in the O-bound κ^1-CO_2 coordinated complex $[((^{Ad}ArO)_3tacn)\text{-}U^{IV}(CO_2^{\bullet-})]$ ($(^{Ad}ArOH)_3$-tacn = 1,4,7-tris(3-adamantyl-5-*tert*-butyl-2-hydroxybenzyl)-1,4,7-triazacyclononane), O–C = 1.122(4) and 1.277(7) Å, with the linear U–O–C and O–C–O bonds stabilized by the sterically encumbering ligand framework.[30,31] Besides, complex **2** displays a significantly longer Ni–O bond distance (2.028(3) Å) than those observed in $[Ni^{II}(L)(pyN_2^{Me2})]^{1-}$ complexes (1.857(5) Å for L = HCO_2^-; 1.817(4) Å for L = HCO_3^-).[32]

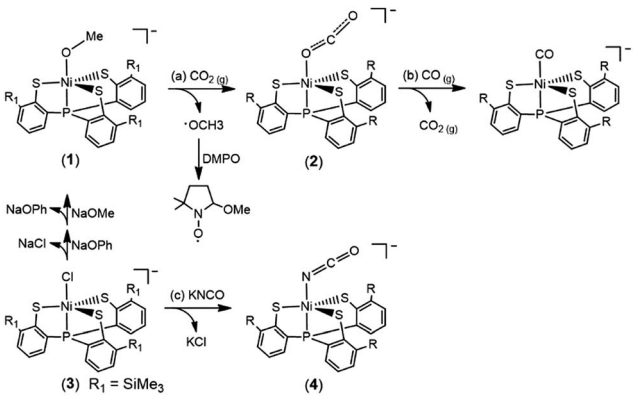

Scheme 1

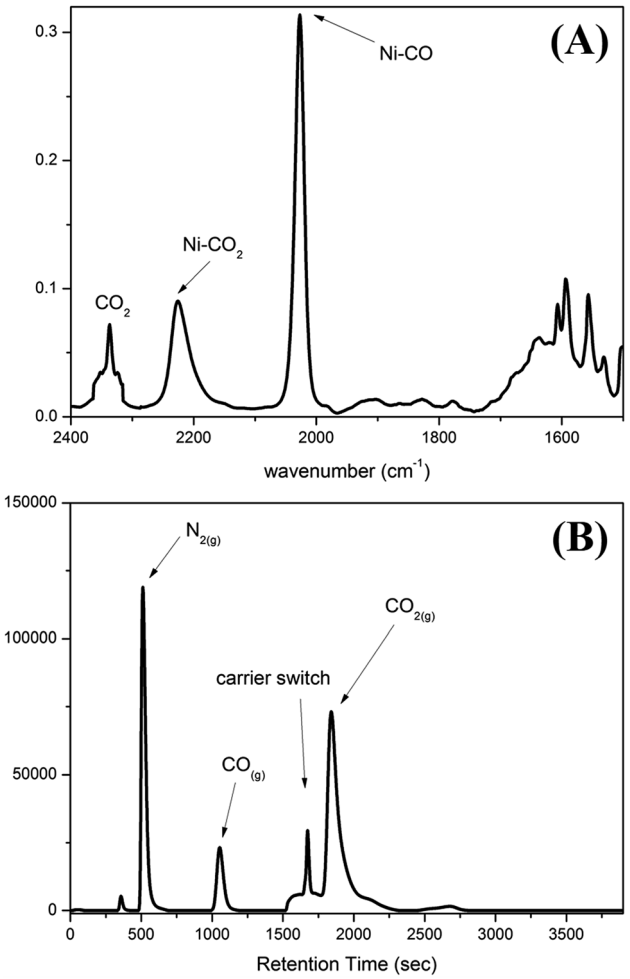

Fig. 1 (A) IR spectra for the transformation of complex **2** to $[Ni^{II}(CO)(PS_3)]^-$ in THF. The decrease in the intensity of the IR ν_{CO_2} peak at 2226 cm^{-1} exhibited by complex **2** with the simultaneous formation of an IR ν_{CO} peak at 2027 cm^{-1} indicated the formation of complex $[Ni^{II}(CO)(PS_3)]^-$. (B) GC chromatogram, derived from the sample collected from the headspace of the tube containing the reaction solution of complex **2** and $CO_{(g)}$, indicating the release of $CO_{2(g)}$ during the transformation of complex **2** to $[Ni^{II}(CO)(PS_3)]^-$.

X-ray absorption/emission spectrum

A Ni and S K-edge X-ray absorption spectroscopic (XAS) study of complex **2** was further attempted to investigate its electronic structure using complexes **1** and **4** as reference complexes. As shown in Fig. 3A, the Ni K-edge XAS of complex **2** (8333.1 eV) together with analogous complexes **1** (8332.9 eV) and **4** (8332.7 eV) shows a similar Ni_{1s}-to-Ni_{3d} transition energy. Accordingly, the

Open Access Article. Published on 24 February 2016. Downloaded on 06/05/2016 19:23:44.
This article is licensed under a Creative Commons Attribution 3.0 Unported Licence.

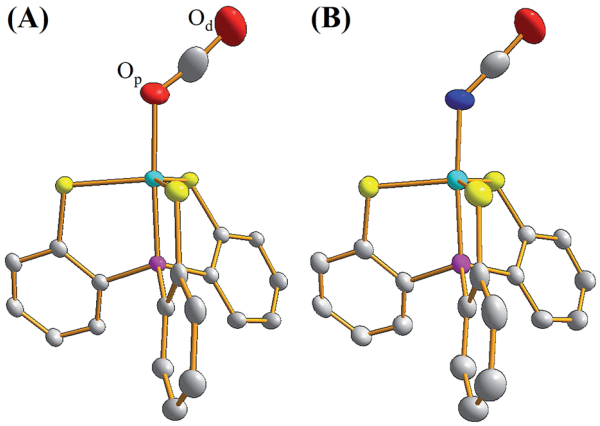

Fig. 2 ORTEP drawing schemes of (A) complex **2** and (B) complex **4** with thermal ellipsoids drawn at a 50% probability level. The Ni, P, S, O, N, and C atoms are shown as light blue, purple, yellow, red, blue, and white ellipsoids. The H atom and TMS group are omitted for clarity. Selected bond distances (Å) and angles (°) for complex **2**: Ni–O_p, 2.028(3); Ni–P, 2.122(1); Ni–S, 2.221(1), 2.287(1), and 2.285(1); O_p–C, 1.132(6); O_d–C, 1.240(7); O–Ni–P, 176.2(1); Ni–O–C, 127.0(4); O_p–C–O_d, 171.7(7). Selected bond distances (Å) and angles (°) for complex **4**: Ni–N, 1.933(2); Ni–P, 2.120(1); Ni–S, 2.226(1), 2.286(1), and 2.291(1); O–C, 1.200(3); N–C, 1.181(3); N–Ni–P, 175.0(1); Ni–N–C, 135.1(2); O–C–N, 177.2(3).

formal oxidation state of Ni in complex **2** is similar to those of complexes **1** and **4**, which are generally known as a L ligand bound to a d^7 Ni(III) center in $[Ni^{III}(L)(PS_3)]^-$.[28] Fig. 3B and ESI Fig. S4† depict the S K-edge XAS spectra of complexes **1**, **2**, and **4**, whereas ESI Fig. S5† shows the calculated S K-edge XAS spectra and spectral deconvolution. As shown in Table 1, the intensity-weighted average energy of the S_{1s}-to-Ni_{3d} transitions in combination with the S_{1s}-to-S^*_{C-S} transition energy demonstrate that the Ni_{3d} manifold orbital energy of complex **2** is 0.3 eV higher than those of complexes **1** and **4**.[33,34] With further regard to the Ni_{1s}-to-Ni_{3d} pre-edge transition energy observed in the Ni K-edge XAS, Ni Z_{eff} of complexes **1**, **2**, and **4** are all comparable. That is, the Ni and S K-edge XAS study supports the $[Ni^{III}:CO_2^{\bullet-}]$ electronic structure in complex **2**. As shown in Fig. S6,† the cyclic voltammogram of a 2 mM solution of complex **4** in CH_3CN indicates a reversible interconversion between Ni^{III}/Ni^{II} at $E_{1/2} = -0.58$ V and an irreversible oxidation at $E_{pa} = -0.21$ V, whereas complex **2** exhibits a reversible interconversion between Ni^{III}/Ni^{II} at $E_{1/2} = -0.70$ V and an irreversible oxidation at $E_{pa} = -0.29$ V (*vs.* Fc/Fc^+).

With regard to complex **4** as an isolobal equivalent to $[Ni^{III}:CO_2]$, complex **2** is a Ni^{III} complex bearing a 17-valence-electron $[CO_2]^{\bullet-}$ ligand. The significantly lower intensity of the second S_{1s}-to-Ni_{3d} transition peak observed in the S K-edge XAS spectrum of complex **2**, compared to that of complex **4**, discloses that the one extra electron shared by the axial Ni_{3d} orbital and $2\pi_u^*$ orbital of CO_2 leads to a strengthening of the Ni^{III}–$CO_2^{\bullet-}$ bond and stabilizes the coordination of κ^1-$[CO_2]^{\bullet-}$ toward the Ni^{III} center (Fig. 3B and Table 1). As observed in complex $[Ni^{III}(L)(PS_3)]^-$ (L = OMe, SEt, SPh), complex **4** displays an EPR silence at 300 K, an axial signal at $g = 2.27$ and 2.04 at 77 K, and an effective magnetic moment of 1.74 μ_B at 300 K (Fig. 4C and S7A†).[27,28,35] The stabilization of the $[CO_2]^{\bullet-}$ radical through coordination to the Ni^{III} center in complex **2** was further evidenced by EPR spectroscopy.

As shown in Fig. 4A and B, the EPR spectrum of complex **2** at 77 K apparently resembles a combination of the typical EPR signal of $[Ni^{III}(L)(PS_3)]^-$ (g = 2.31, 2.03, and 2.00) and the $[CO_2]^{\bullet-}$ radical with a contribution of Ni_{3d} leading to the observed g anisotropy (Fig. 4A and B).[36] The spin quantitation of complex **2**, using complex **4** as a reference, demonstrates that the electronic structure of complex **2** is best described as a resonance hybrid between $[Ni^{III}:CO_2^{\bullet-}]$ and $[Ni^{II}:CO_2]$, which is supported by the effective magnetic moment of 1.59 μ_B exhibited by complex **2** at 300 K (ESI Fig. S7B and S7C†).

The experimental valence-to-core X-ray emission (V2C XES) spectra of complexes **2** and **4** are presented in Fig. 3C. In comparison with complex **4**, the broad V2C transition peak of complex **2** at 8330.0 eV shifts from 8328.8 eV upon replacement of the $[NCO]^-$ by the $[CO_2]^{\bullet-}$ ligand. DFT calculation was further pursued to verify the nature of the V2C transition(s). As shown in ESI Fig. S8A and S8B,† the DFT calculated V2C XES spectra resembles the experimental V2C features and, in particular, the trend of the energy shift comparing complexes **2** and **4**. The contribution of the $4\sigma_g$, $3\sigma_u$, and $1\pi_g$ orbitals of $[NCO]^-$ and Ni_{3d}–S_{3p} orbitals results in the V2C features of complex **4**.[37] For complex **2**, the absence of transitions from the $3\sigma_u$ and $1\pi_g$ orbitals and an additional transition from the occupied $2\pi_u$

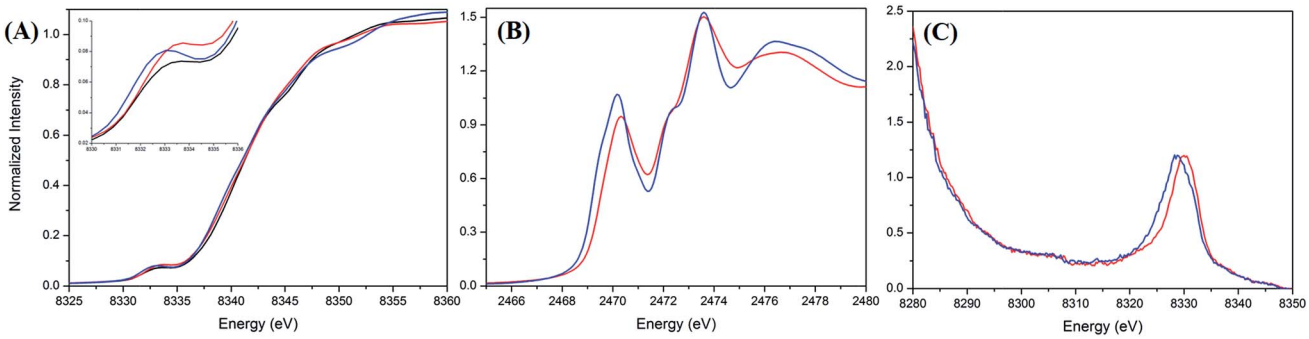

Fig. 3 (A) Ni K-edge X-ray absorption spectra of complexes **1** (black), **2** (red), and **4** (blue). (B) S K-edge X-ray absorption and (C) Ni valence-to-core X-ray emission spectra of complexes **2** (red) and **4** (blue).

Open Access Article. Published on 24 February 2016. Downloaded on 06/05/2016 19:23:44.
This article is licensed under a Creative Commons Attribution 3.0 Unported Licence.

Table 1 $Ni_{1s} \rightarrow Ni_{3d}$, $S_{1s} \rightarrow Ni_{3d}$, $S_{1s} \rightarrow S^{*}_{C-S}$ transition energy and $S_{1s} \rightarrow Ni_{3d}$ transition intensity of complexes **1**, **2**, **4**, and $[Ni(SPh)(PS_3)]^-$, derived from the Ni and S K-edge X-ray absorption spectroscopy

Complexes	$Ni_{1s} \rightarrow Ni_{3d}$ energy[a] (eV)	$S_{1s} \rightarrow Ni_{3d}$ energy[b] (eV)			$S_{1s} \rightarrow Ni_{3d}$ intensity[b]		$S_{1s} \rightarrow S^{*}_{C-S}$ energy[b] (eV)	Relative d-manifold energy shift[d] (eV)
		1st peak	2nd peak	Avg[c]	1st peak	2nd peak		
1	8332.9	2469.7	2470.4	2470.0	0.29	1.34	2472.1	0
2	8333.1	2469.9	2470.5	2470.3	0.47	1.15	2472.1	0.3
4	8332.7	2469.5	2470.2	2470.1	0.33	1.77	2472.2	0
$[Ni(SPh)(PS_3)]^-$	8333.0	2469.8	2470.4	2470.3	0.52	1.91	2472.3	0.1

[a] The peak energy is determined by the minimum of the second derivative. [b] The peak energy and intensity is determined based on the spectral deconvolution. [c] The intensity-weighted average energy is given here. [d] Calculated from the difference of the thiolate peak energy and the intensity-weighted pre-edge peak energy.

orbital of $[CO_2]^{\bullet -}$, in addition to the upward shift of the Ni_{3d}–S_{3p} orbitals in complex **2**, rationalizes the higher V2C transition energy of complex **2** in comparison with complex **4**.

Complex $[Ni(L)(P(C_6H_3\text{-}3\text{-}SiMe_3\text{-}2\text{-}S)_3)]^-$, embedded in a distorted trigonal bipyramidal geometry, features a wealth of chemical reactivity tailored by the oxidation state of Ni and coordinating ligand L (L = OPh, SPh, SePh and Cl for Ni^{III}; L = CO, N_2H_4 for Ni^{II}).[27,28,35] To dissect the unique reactivity of $[Ni^{III}(OMe)(PS_3)]^-$ (**1**) toward CO_2 activation, the addition of CO_2 into a THF solution of the representative Ni^{III}-chalcogenate complex $[Ni(SPh)(PS_3)]^-$ was investigated. In contrast to the reaction of complex **1** and CO_2 yielding complex **2**, complex $[Ni^{III}(SPh)(PS_3)]^-$ is inert toward CO_2. In addition, despite the potential reduction power of the Ni^{II} center in combination with the labile nature of the CO or N_2H_4 ligand, neither complex $[Ni^{II}(CO)(PS_3)]^-$ nor complex $[Ni^{II}(N_2H_4)(PS_3)]^-$ showed a reactivity toward CO_2 when the THF solution of these Ni complexes was treated with CO_2, respectively, at ambient temperature for 3 days. As shown in ESI Fig. S4† and Table 1, the covalent character of the $[Ni^{III}(SPh)]$ core, compared to the $[Ni^{III}(OMe)]$ core, derived from the σ-/π-electron-donating nature of the coordinated phenylthiolate ligand, rationalizes the inertness of $[Ni^{III}(SPh)(PS_3)]^-$ toward CO_2.[33,34] Despite the labile nature of CO and N_2H_4, the inert reactivity of the Ni^{II} center toward CO_2 demonstrates that the lowered Ni_{3d} manifold orbitals in Ni^{III} complex **1** attracts the binding of weak σ-donor CO_2 and triggers the subsequent reduction of CO_2 by the nucleophilic $[OMe]^-$ in the immediate vicinity. The reactivity of complex **1** toward CO_2, affording an O-bound $[Ni^{III}{:}CO_2^{\bullet -}]$ species, uncovers a novel strategy for the immobilization and reductive activation of CO_2, contrary to the typical interaction of unoccupied CO_2 $2\pi^{*}_{u}$ orbitals with filled high-lying metal d orbitals in low-valence metal complexes.[38,39] Theoretically, lowering the energy of the $2\pi^{*}_{u}$ ($6a_1$) (LUMO) orbital on CO_2 for interaction with nickel orbitals binding by way of the O=C– unit may be responsible for the coordinated CO_2 reduction and the nonlinearity of the triatomic CO_2 molecule which contains 17 valence electrons, as reported by McGlynn and co-workers.[37] These results illustrate aspects of how a coordinated ligand and the electronic state of the nickel center work in concert to trigger coordination and activation of CO_2.

Conclusions

Complex **1**, with the inherent combination of an electrophilic $[Ni^{III}(PS_3)]$ core and a properly positioned $[OMe]^-$ nucleophile, was employed to provide an optimum electronic condition to trap and activate CO_2 to afford complex **2**, containing the O-coordinated $[\kappa^1\text{-}CO_2]^{\bullet -}$ ligand. The Ni^{III}-mediated reduction of CO_2 by an adjacent $[OMe]^-$ ligand immobilizes CO_2 in the form of $[Ni^{III}{:}CO_2^{\bullet -}]$ and may open a novel CO_2 activation pathway promoting the subsequent incorporation of CO_2 in the buildup of functionalized products.

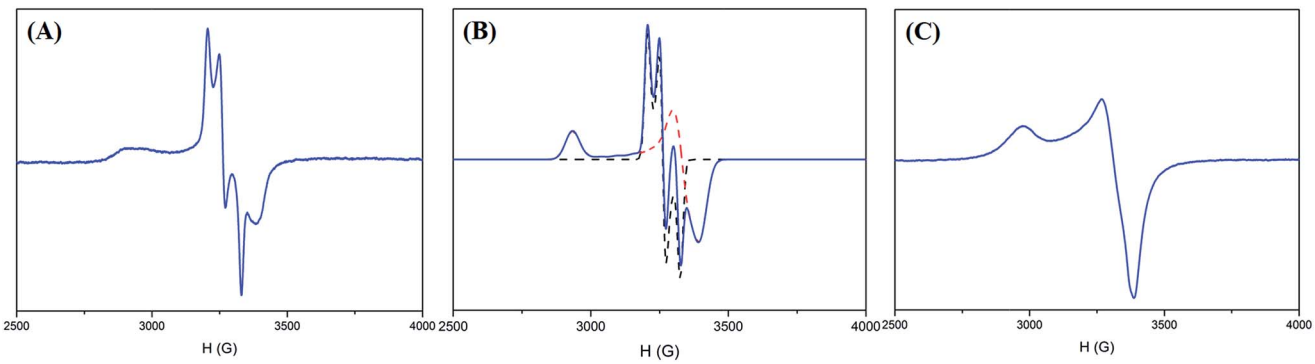

Fig. 4 (A) EPR spectrum of complex **2** at 77 K, (B) simulated EPR spectrum (blue) of complex **2** combining $[Ni^{III}(L)(PS_3)]^-$ (dashed red line) and the $[CO_2]^{\bullet -}$ radical (dashed black line), and (C) EPR spectrum of complex **4** at 77 K.

This journal is © The Royal Society of Chemistry 2016

Open Access Article. Published on 24 February 2016. Downloaded on 06/05/2016 19:23:44.
This article is licensed under a Creative Commons Attribution 3.0 Unported Licence.

Acknowledgements

We gratefully acknowledge the support on the hardware and software from staff at BL-16A and BL-17C of NSRRC, and BL 6-2 of SLAC. Authors thank Ms Pei-Lin Chen for single-crystal X-ray structural determinations, Mr Yu-Huan Lu and Prof Hsin-Tsung Chen for the help on theoretical calculation. We also thank the Ministry of Science and Technology (Taiwan) for the financial support.

Notes and references

1 T. Sakakura, J. C. Choi and H. Yasuda, *Chem. Rev.*, 2007, **107**, 2365.
2 D. J. Darensbourg, *Chem. Rev.*, 2007, **107**, 2388.
3 J.-H. Jeoung and H. Dobbek, *Science*, 2007, **318**, 1461.
4 M. Can, F. A. Armstrong and S. W. Ragsdale, *Chem. Rev.*, 2014, **114**, 4149.
5 J. Fesseler, J.-H. Jeoung and H. Dobbek, *Angew. Chem.*, 2015, **54**, 8560.
6 M. Aresta, C. F. Nobile, V. G. Albano, E. Forni and M. Manassero, *J. Chem. Soc., Chem. Commun.*, 1975, 636.
7 J. S. Anderson, V. M. Iluc and G. L. Hillhouse, *Inorg. Chem.*, 2010, **49**, 10203.
8 Y.-E. Kim, J. Kim and Y. Lee, *Chem. Commun.*, 2014, **50**, 11458.
9 Y.-E. Kim, S. Oh, S. Kim, O. Kim, J. Kim, S. W. Han and Y. Lee, *J. Am. Chem. Soc.*, 2015, **137**, 4280.
10 C. Costentin, M. Robert and J. M. Saveant, *Chem. Soc. Rev.*, 2013, **42**, 2423.
11 M. Aresta and A. Dibenedetto, *Dalton Trans.*, 2007, 2975.
12 A. Looney, R. Han, K. Mcneill and G. Parkin, *J. Am. Chem. Soc.*, 1993, **115**, 4690.
13 O. R. Allen, S. J. Dalgarno, L. D. Field, P. Jensen, A. J. Turnbull and A. C. Willis, *Organometallics*, 2008, **27**, 2092.
14 A. Jana, D. Ghoshal, H. W. Roesky, I. Objartel, G. Schwab and D. Stalke, *J. Am. Chem. Soc.*, 2009, **131**, 1288.
15 S. F. Yin, J. Maruyama, T. Yamashita and S. Shimada, *Angew. Chem.*, 2008, **47**, 6590.
16 B. Kersting, *Angew. Chem.*, 2001, **40**, 3987.
17 M. Vogt, A. Nerush, Y. Diskin-Posner, Y. Ben-David and D. Milstein, *Chem. Sci.*, 2014, **5**, 2043.
18 G. A. Filonenko, M. P. Conley, C. Copéret, M. Lutz, E. J. M. Hensen and E. A. Pidko, *ACS Catal.*, 2013, **3**, 2522.
19 C. C. Lu, C. T. Saouma, M. W. Day and J. C. Peters, *J. Am. Chem. Soc.*, 2007, **129**, 4.
20 M. T. Whited and R. H. Grubbs, *J. Am. Chem. Soc.*, 2008, **130**, 5874.
21 B. C. Fullmer, H. J. Fan, M. Pink and K. G. Caulton, *Inorg. Chem.*, 2008, **47**, 1865.
22 I. Castro-Rodriguez and K. Meyer, *J. Am. Chem. Soc.*, 2005, **127**, 11242.
23 S. C. Bart, C. Anthon, F. W. Heinemann, E. Bill, N. M. Edelstein and K. Meyer, *J. Am. Chem. Soc.*, 2008, **130**, 12536.
24 J. G. Rebelein, Y. Hu and M. W. Ribbe, *Angew. Chem.*, 2014, **53**, 11543.
25 R. Angamuthu, P. Byers, M. Lutz, A. L. Spek and E. Bouwman, *Science*, 2010, **327**, 313.
26 G. H. Jin, C. G. Werncke, Y. Escudiee, S. Sabo-Etienne and S. Bontemps, *J. Am. Chem. Soc.*, 2015, **137**, 9563.
27 T.-W. Chiou and W.-F. Liaw, *Inorg. Chem.*, 2008, **47**, 7908.
28 C.-M. Lee, Y.-L. Chuang, C.-Y. Chiang, G.-H. Lee and W.-F. Liaw, *Inorg. Chem.*, 2006, **45**, 10895.
29 N. A. M. Azman, S. Peiro, L. Fajari, L. Julia and M. P. Almajano, *J. Agric. Food Chem.*, 2014, **62**, 5743.
30 I. Castro-Rodriguez, H. Nakai, L. N. Zakharov, A. L. Rheingold and K. A Meyer, *Science*, 2004, **305**, 1757.
31 W. J. Evans, C. A. Seibel and J. W. Ziller, *Inorg. Chem.*, 1998, **37**, 770.
32 D. G. Huang and R. H. Holm, *J. Am. Chem. Soc.*, 2010, **132**, 4693.
33 T.-T. Lu, S.-H. Lai, Y.-W. Li, I.-J. Hsu, L.-Y. Jang, J.-F. Lee, I.-C. Chen and W.-F. Liaw, *Inorg. Chem.*, 2011, **50**, 5396.
34 E. I. Solomon, B. Hedman, K. O. Hodgson, A. Dey and R. K. Szilagyi, *Coord. Chem. Rev.*, 2005, **249**, 97.
35 C.-M. Lee, C.-H. Chen, S.-C. Ke, G.-H. Lee and W.-F. Liaw, *J. Am. Chem. Soc.*, 2004, **126**, 8406.
36 J. H. Lunsford and J. P. Jayne, *J. Phys. Chem.*, 1965, **69**, 2182.
37 J. W. Rabalais, J. M. Mcdonald, V. Scherr and S. P. Mcglynn, *Chem. Rev.*, 1971, **71**, 73.
38 X. L. Yin and J. R. Moss, *Coord. Chem. Rev.*, 1999, **181**, 27.
39 D. H. Gibson, *Chem. Rev.*, 1996, **96**, 2063.